Chapter 4

APPLICATION OF ELECTRIC VEHICLES FOR FREQUENCY REGULATION USING SOC-BASED V2G CONTROLLER

4.1 INTRODUCTION

There has been a significant increase in adapting green technologies for power production to de-carbonize the electric power system and transport system as well. This further aids in the conservation of the fast-depleting non-renewable energy sources, i.e. fossils. In this context, there has been growing interest in Electric Vehicles (EVs) in recent years, as shown in Fig. 4.1. The widespread adoption of EVs can pose a serious challenge to the power system operation whereas, on the contrary, they can prove to be a great opportunity with requisite control schemes. Some studies have shown the impact of EVs on power systems while considering them as regular loads. The significant conclusion of these studies remarks the controllability over the EV charging loads to allow higher integration of EVs without disturbing the optimal power system operation.

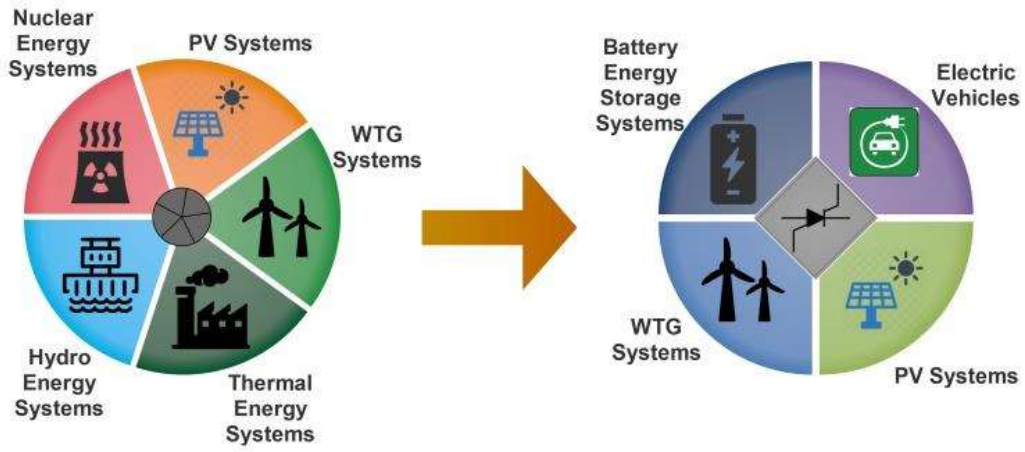

Fig. 4.1 Evolution of power systems from conventional energy sources to the integration of renewable energy sources.

As a consequence of large-scale development in smart charging schemes, the capability of EVs is being utilized to assist Independent System Operators (ISO) in frequency regulation by adjusting their real-time charging and discharging power in accordance with the Area Control Error (ACE) signal.

In this study, two controllers (grid regulation and charger controller) are suggested by taking into account various charging profiles and the battery state of charge for electric vehicles. These controllers offer bidirectional power flow, which can serve as primary frequency control under various contingencies across a 24-hour period. The proposed controller can effectively mitigate the frequency deviations and control power interchange in the tie-line between interconnected systems. A Transient Frequency Deviation Index (TFDI) is used to estimate the severity of the contingency on frequency variations. In the presented cases, the frequency deviation is within the limits of critical frequency. However, a significant improvement in the security margin is observed while EVs provide ancillary services, i.e. grid frequency regulation.

4.2 SYSTEM MODELLING AND SOLUTION METHODOLOGY

As discussed in Section 4.1. this work evaluates the utilization of EVs for frequency regulation in an interconnected two-area system. A typical setup of a micro-grid with an EV fleet is shown in Fig. 4.2. Two stages of disturbance have been considered in this research. In the first case, a line-to-ground fault was simulated, whereas, in the second scenario, reference power to the Steam Turbine Governor (STG) was reduced to simulate disturbance. To investigate the two cases, the adopted methodology is as follows:

1. The two-area system model was characterized in terms of generation, load and electricity grid.

2. For the disturbances mentioned above, a simulation is carried out for cases where EVs are disconnected from the grid.

3. The same simulation was carried out when EVs are grid-connected and participate in frequency regulation.

Further, observations on power system frequency response are made based on the results obtained from the simulations.

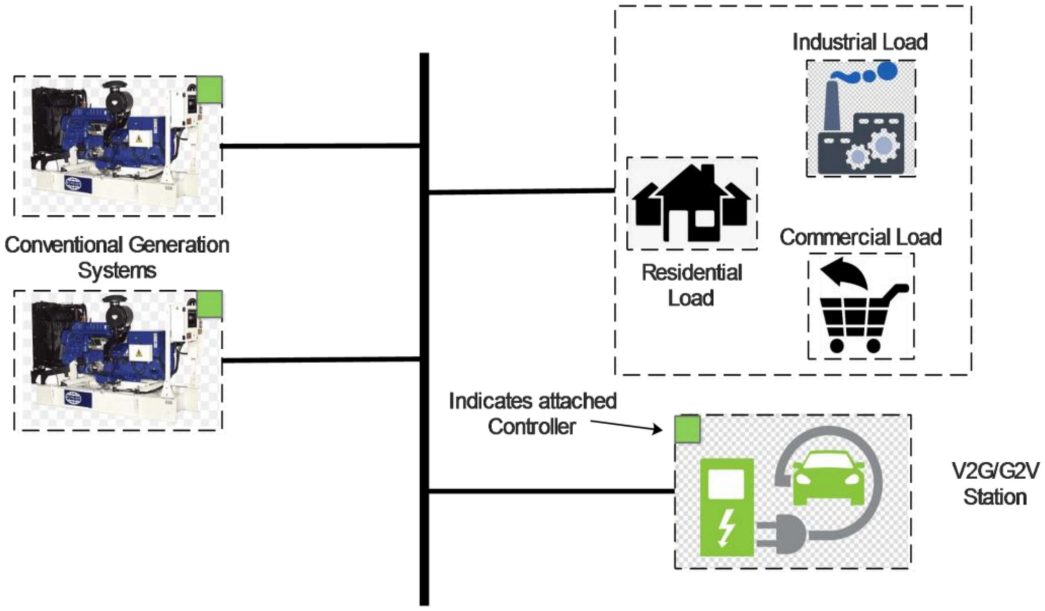

Fig. 4.2 Structure of grid with an attached EV charging station.

4.2.1 Power system network modelling

The 11-bus two-area system [101] was modelled using SIMULINK in MATLAB with the parameters specified in Table 4.1. A detailed model of the power system network was created consisting of generation units, loads and electricity grid while taking characteristics of generation unit and their response to drops in frequency into consideration. The single diagram of the network is shown in Fig. 4.3.

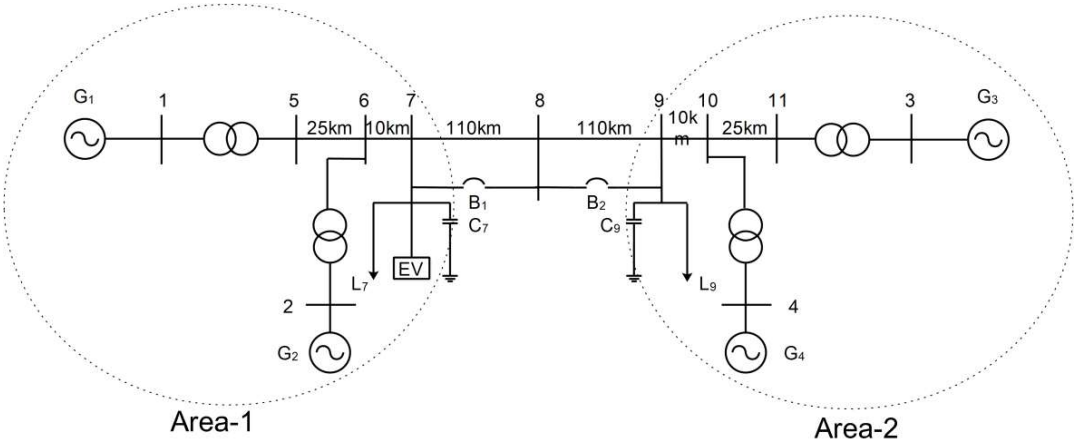

Fig. 4.3 Single-line diagram of the modified two-area system.

Table 4.1 Parameters of the power system network.

Area-1		Area-2	
Parameter	Specification	Parameter	Specification
Synchronous Generator, G_1	900MVA	Synchronous Generator, G_3	900MVA
Synchronous Generator, G_2	900MVA	Synchronous Generator, G_4	900MVA
Load, L_7	967MW, 100MVAR	Load, L_9	1767MW, 100MVAR
Static Capacitor, C_7	200MVAR	Static Capacitor, C_9	350MVAR

The generator unit model is classified based upon the order of complexity and is modelled in accordance with the same. It is a two-axis model with damper windings and excitation windings in the d-axis. The following derived equations represent first order mathematical model of a synchronous machine:

Stator voltage equations in *dq0* components

$$e_d = \frac{d\Psi_d}{dt} - \Psi_q \frac{d\theta}{dt} - R_a i_d$$

$$e_q = \frac{d\Psi_q}{dt} + \Psi_d \frac{d\theta}{dt} - R_a i_q \tag{4.1}$$

$$e_0 = \frac{d\Psi_0}{dt} - R_a i_0$$

with stator flux linkages

$$\Psi_d = -(L_{aa0} + L_{ab0} + \frac{3}{2}L_{aa2})i_d + L_{afd}i_{fd} + L_{akd}i_{kd}$$

$$\Psi_q = -(L_{aa0} + L_{ab0} - \frac{3}{2}L_{aa2})i_q + L_{akq}i_{kq} \tag{4.2}$$

$$\Psi_0 = -(L_{aa0} - 2L_{ab0})i_0$$

and rotor voltage equations in *dq0* components

$$e_{fd} = \frac{d\Psi_{fd}}{dt} + R_{fd}i_{fd}$$

$$0 = \frac{d\Psi_{kd}}{dt} + R_{kd}i_{kd} \tag{4.3}$$

$$0 = \frac{d\Psi_{kq}}{dt} + R_{kq}i_{kq}$$

with rotor flux linkages

$$\Psi_{fd} = L_{ffd}i_{fd} + L_{fkd}i_{kd} - \frac{3}{2}L_{afd}i_d$$

$$\Psi_{kd} = L_{fkd}i_{fd} + L_{kkd}i_{kd} - \frac{3}{2}L_{akd}i_d \tag{4.4}$$

$$\Psi_{kq} = L_{kkq}i_{kq} - \frac{3}{2}L_{akq}i_q$$

Torque and power equations can be derived from the above equations as:

$$P_t = \frac{3}{2}[(i_d p\Psi_d + i_q p\Psi_q + 2i_0 p\Psi_0) + (i_q\Psi_d - i_d\Psi_q)\omega_r - R_a(i_d^2 + i_q^2 + 2i_0^2)] \quad (4.5)$$

$$T_e = \frac{3}{2}\frac{P}{2}(\Psi_d i_q - \Psi_q i_d) \quad (4.6)$$

The following notations have been used in writing the above equations:

e_d, e_q, e_0	=	stator voltages in *dq0* components
i_d, i_q, i_0	=	stator currents in *dq0* components
e_{fd}	=	field voltage
i_{fd}, i_{kd}, i_{kq}	=	field and amortisseur circuit current
R_{fd}, R_{kd}, R_{kq}	=	rotor circuit resistance
L_{aa}, L_{bb}, L_{cc}	=	self-inductances of stator windings
L_{ab}, L_{bc}, L_{ca}	=	mutual inductances between stator windings
$L_{afd}, L_{akd}, L_{akq}$	=	mutual inductances between stator and rotor windings
$L_{ffd}, L_{kkd}, L_{kkq}$	=	self-inductances of rotor windings
R_a	=	armature resistance per phase
p	=	differential operator, $\frac{d}{dt}$
P_t	=	three phase power output of the synchronous generator
T_e	=	developed electrical torque in synchronous generator

The loads are represented as a Constant Power model, the transmission lines are represented by equivalent π-model, whereas transformers are represented as series impedances.

4.2.2 EV modelling

In the present research, aggregated EV model is used to study its impact on the described 11-bus power system network. The State of Charge (SOC) for various EV profiles is

initialized based on the driving patterns of the EV owner and charging availability at parking. Further, the values of SOC are updated based on their plug-in state and charge-discharge status calculated using equation (4.7) given below.

SOC of k^{th} class of EVs is given by,

$$SOC_k = \begin{cases} \frac{1}{N_{bcars\,k}} \int_0^t \frac{P_{charg}}{N_{bcharg}} \times N_{bcars\,k}\,, & charge = 1 \\ \frac{1}{N_{bcars\,k}} \int_0^t \frac{P_{reg}}{N_{breg}} \times N_{bcars\,k}\,, & charge = 0 \end{cases} \tag{4.7}$$

$$with \;\; SOC_k(0) = SOC_{k\,initial} \times N_{bcars\,k}$$

where, $N_{bcars\,k}$ is the no. of EVs in class k, P_{charg} is the total power available in charging mode and N_{bcharg} is the no. of grid-connected EVs in charging mode. P_{reg} is the total power available in frequency regulation mode and N_{breg} is the no. of grid-connected EVs in regulation mode.

The charge-discharge decision of EVs is based upon the SOC and plug state, as shown in Fig. 4.4. The SOC value of each EV Profile is compared with the SOC limits of 85-95% for frequency regulation. These signals are input to the S-R latch. When SOC ≤ 85%, the latch is SET, and EV is in charging mode. For 85% ≤ SOC ≤ 95%, the latch is RESET, and EV is in frequency regulation mode. However, the EV must be plugged into the charging station in both cases.

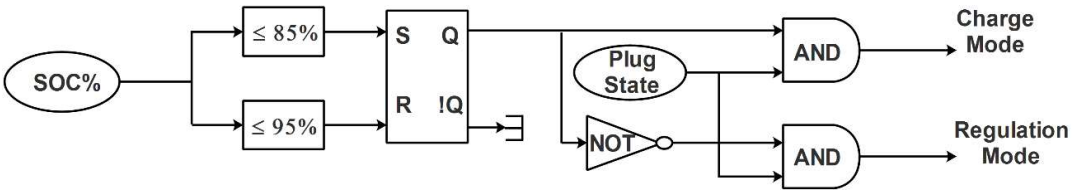

Fig. 4.4 Control logic for the charge-discharge decision of EVs.

In the frequency regulation mode of EV, regulation power is calculated based on the frequency deviation limits of -0.5×10^{-3} Hz to 0.5×10^{-3} Hz (where the – sign

indicates a drop in frequency, whereas the + sign indicates frequency rise) and is given by,

$$P_{reg} = \begin{cases} \int_0^t \left[K_D \times \frac{d(\omega_{ref} - \omega_{sys})}{dt} + K_P \times (\omega_{ref} - \omega_{sys}) \right] \\ \qquad for -P_{max\,reg} < P_{reg} < P_{max\,reg} \\ P_{max\,reg}, \\ \qquad for\ P_{reg} \geq P_{max\,reg} \\ -P_{max\,reg}, \\ \qquad for\ P_{reg} \leq -P_{max\,reg} \end{cases} \tag{4.8}$$

where, P_{reg} is the power injected/absorbed by the EV fleet in regulation mode, K_D and K_P are the gains of the derivative and proportional controller, respectively, ω_{ref} and ω_{sys} are the nominal and actual system frequency and $P_{max\,reg}$ is the maximum power limit of the EV fleet in regulation mode.

The system frequency (in p.u.), measured at bus 7, is compared with the frequency reference, i.e. 1 p.u. The error signal so generated is checked for frequency violation limits. During an under-frequency event, if the frequency falls more than 0.5×10^{-3} Hz or in an over-frequency event, if the frequency rises more than 0.5×10^{-3} Hz from the reference, the error signal is passed through the OR block as shown in Fig. 4.5. The simulation time is generated from the clock, and the signal is AND with an error signal. The selector switch passes the obtained signal if it is greater than the threshold value, i.e. zero in this case, and it passes zero if the signal is less than or equal to the threshold value. The obtained signal is input to the Proportional-Derivate (PD) controller with the gains specified in Table 4.2, and further, the signal is integrated over the period of deviation. The saturation block limits the power injection/absorption based on the maximum power available for the regulation $P_{max\,reg}$.

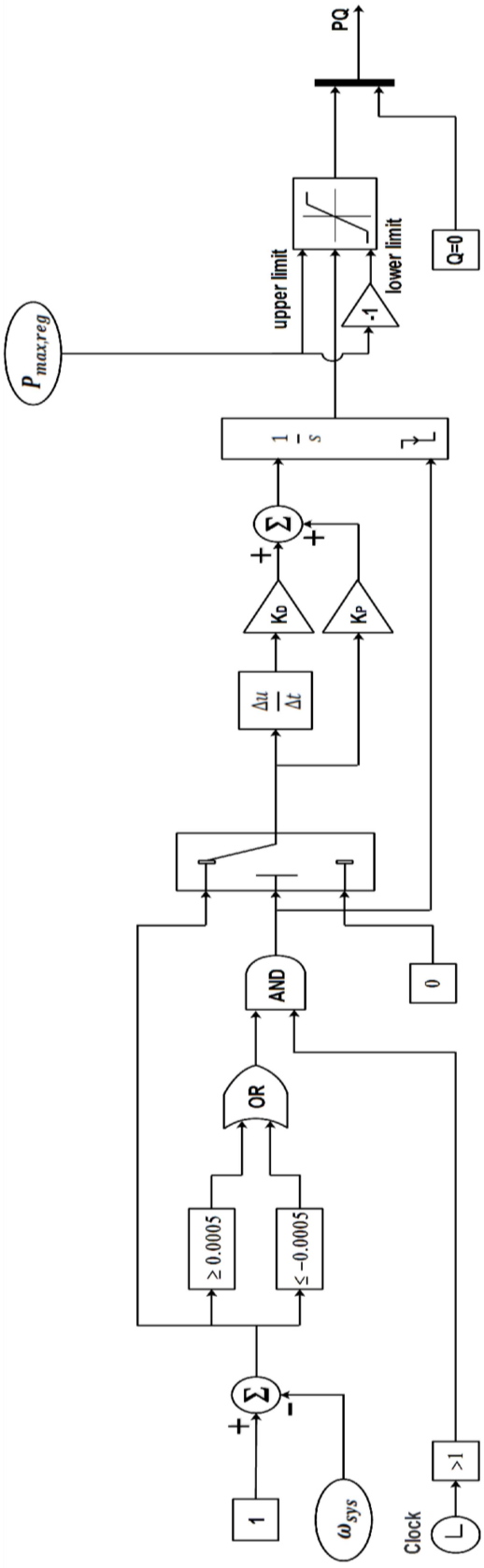

Fig. 4.5 Control block-diagram for power regulation through EV fleet.

Table 4.2 Parameters of the EV fleet.

Parameter	Specification
Rated Capacity	20MW
System Efficiency	90%
Number of EVs in Class 1	175
Number of EVs in Class 2	125
Number of EVs in Class 3	50
Number of EVs in Class 4	100
Number of EVs in Class 5	50
Derivative Controller Gain, K_D	2
Proportional Controller Gain, K_P	4000

The individual EVs were classified based upon the availability of charging and their driving pattern as:

Class 1: EV owners going to work with charging available at parking.

Class 2: EV owners going to work with long drives with charging available at parking.

Class 3: EV owners going to work with no charging facility available at parking.

Class 4: EV owners residing at home.

Class 5: EV owners going to work in night shifts.

These five classes have been divided into sub-categories of five each. This categorization is based upon the battery capacity of the EV available in the market, as shown in Table 4.3.

Table 4.3 Characterization of the EV fleet.

Classification based upon EV owner's driving pattern	No. of EVs	No. of EVs based upon battery size				
		Type 1 (18.55kWh)	Type 2 (44.8kWh)	Type 3 (30.2kWh)	Type 4 (100kWh)	Type 5 (100kWh)
Class 1	175	67	32	47	10	19
Class 2	125	61	14	25	12	13
Class 3	50	15	12	16	3	4
Class 4	100	37	16	30	10	7
Class 5	50	18	10	14	5	3

4.2.3 Transient Frequency Deviation Index (TFDI)

A frequency deviation index [102] is used to assess the severity of the frequency transient. The relationship between the system frequency response curve and critical frequency can be expressed based upon whether the minimum system frequency within the observed window is less than or equal to critical frequency or minimum frequency deviation is greater than the critical frequency in the observed window.

Case A: Intersection exists

As shown in Fig. 4.6, two intersection points of critical frequency exist with the system frequency curve. Three different cases may arise depending upon inequality/equality conditions between t_b, the time interval for which frequency is less than the critical value and t_{cr}, time duration for which observation is made. The expression for TFDI is given by:

$$\eta = \frac{t_{cr} - t_b}{t_{cr}} \tag{4.9}$$

$t_b < t_{cr}$, breakdown time is less than critical time, and η is positive.

$t_b = t_{cr}$, break down time is equal to the critical time and $\eta = 0$, which implies the critical security situation.

$t_b > t_{cr}$, breakdown time is greater than critical time, and η is negative, which refers to broken security.

In the above-mentioned case, security assessment can be carried out based on the time difference between t_b and t_{cr}. However, this index cannot strictly determine the degree of severity for the cases when there is no intersection between the system frequency curve and critical frequency, i.e. when $t_b = 0$.

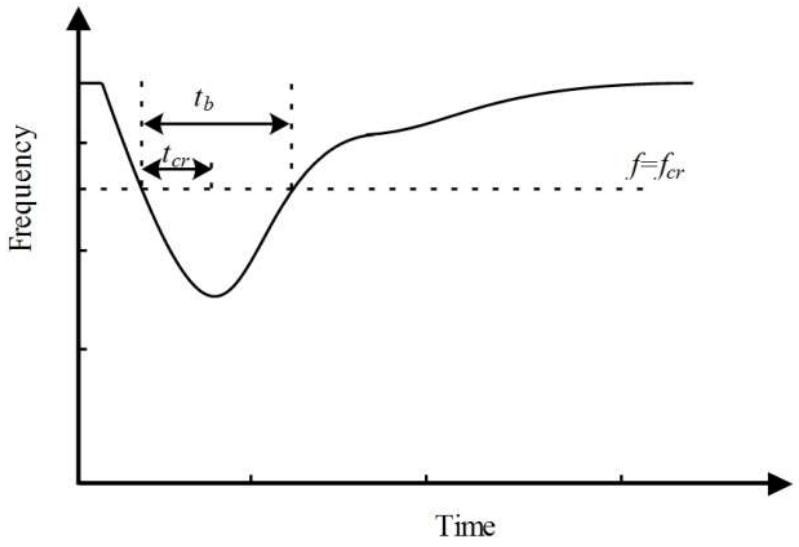

Fig. 4.6 Frequency response curve having intersection with line $f = f_{cr}$.

Case B: Intersection does not exist

There is no intersection between the system frequency curve and critical frequency i.e. f_{min} is always greater than f_{cr} as shown in Fig. 4.7, and hence, system security cannot be evaluated from the time perspective. Thus, in this case, a security index is formulated

considering the difference between f_{min} and f_{cr}. To maintain consistency with the security index presented in Case A, the modified security index is given by:

$$\eta = \frac{f_{min} - f_{cr}}{f_N - f_{cr}} + 1 \tag{4.10}$$

where, f_N is the nominal system frequency.

When f_{min} is equal to f_{cr}, i.e. there is only one cross-point between the system frequency curve and f_{cr}, TFDI $\eta = 1$. Since $f_{cr} \leq f_{min} \leq f_N$, the modified security index η lies between values 1 and 2, i.e. $1 \leq \eta \leq 2$.

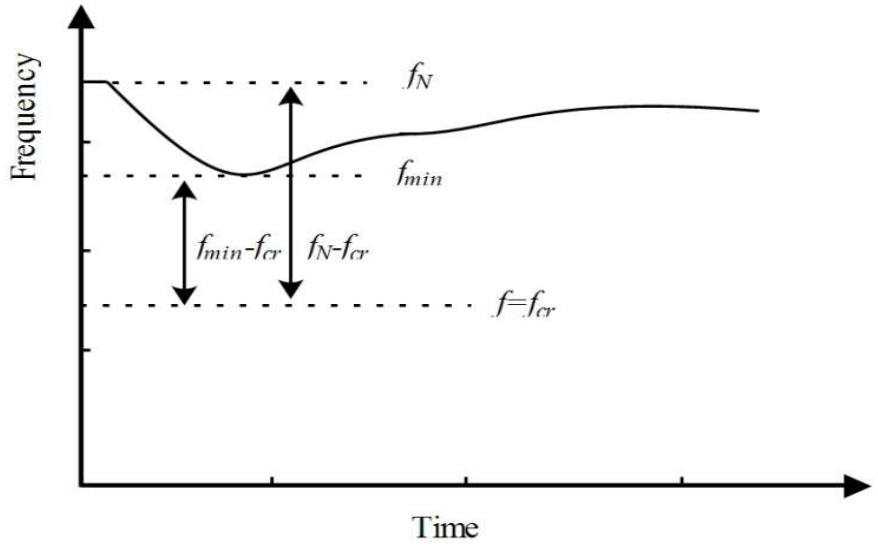

Fig. 4.7 Frequency response curve having no intersection with line $f = f_{cr}$.

4.3 PROBLEM FORMULATION

The grid operators control the output of the generating units based on ACE for frequency regulation and absorbing the fluctuations in an area. In this work, ACE is dispatched to the EV fleet in the area to restore the frequency to the nominal value and maintain the tie-line power to the desired value. The block diagram for the two-area frequency control

system corresponding to the 11-bus network considered in this work is shown in Fig. 4.8. An EV fleet is connected at bus 7 in Area-1 and is shown as a negative load with a '+' sign in Area-1. The power drawn by EV load is either positive or negative depending upon whether EVs draw a net charging power or have a net discharging power into the grid. The EV fleet is modelled as a Proportional-Derivative controller in cascade with an integrator that takes frequency deviation of Area-1 as input and injects/draws power as per ACE based on SOC of EVs. In the interconnected power system, to minimize the frequency deviation, ACE has been defined as:

$$ACE_i = \Delta P_i + \beta_i \Delta f_i \tag{4.11}$$

$$\text{with } \beta_i = D_i + \frac{1}{R_i}$$

where, Δf_i is frequency deviation in Area-i in p.u., ΔP_i is the net change in the power injected from Area-i to all other areas through tie-lines in p.u., β_i is the frequency bias of Area-i, R_i is the governor droop for Area-i, D_i is the damping coefficient for the power system in Area-i.

This work has considered a two-area system; ACEs for two areas are given by:

$$ACE_1 = \Delta P_{12} + \beta_1 \Delta f_1 \tag{4.12}$$

$$ACE_2 = \Delta P_{21} + \beta_2 \Delta f_2 \tag{4.13}$$

$$\Delta P_{12} = -\Delta P_{21} \tag{4.14}$$

where, ACE_1 is the Area Control Error for Area-1, ACE_2 is the Area Control Error for Area-2, ΔP_{12} is the power injected into the tie-line from Area-1, $\Delta P_{21} = -\Delta P_{12}$ is the power injected into the tie-line from Area-2, Δf_1 is frequency deviation in Area-1, Δf_2 is

frequency deviation in Area-2, β_1 is frequency bias factor for Area-1 and β_2 is frequency bias factor for Area-2.

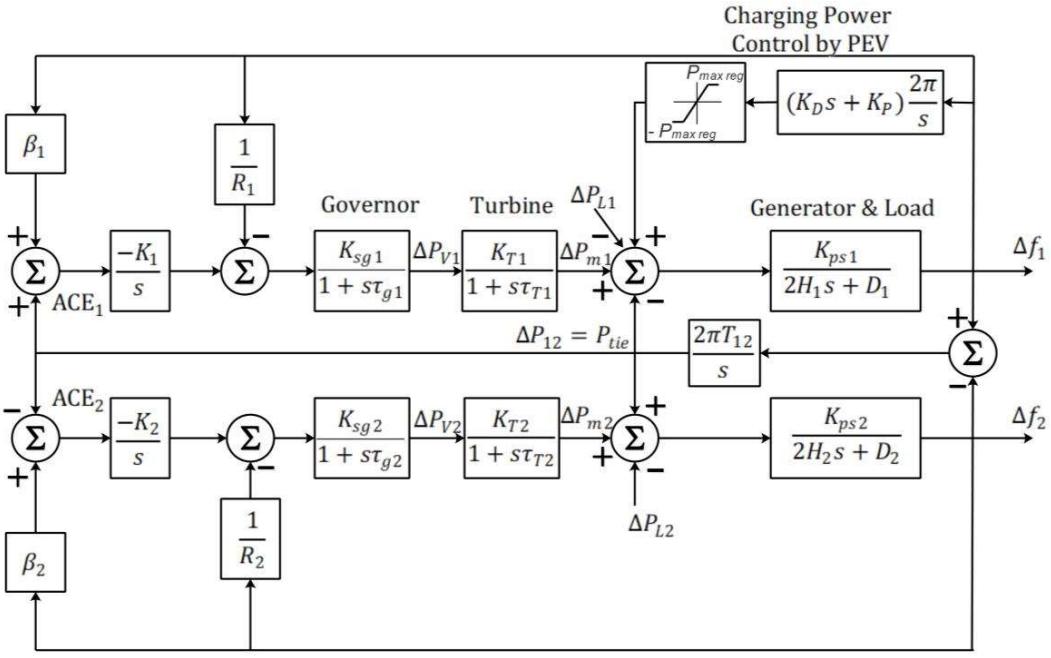

Fig. 4.8 Block diagram of the two-area power system with frequency controls from EV.

Integral Time Absolute Error (ITAE) is chosen for the objective function to be minimized as it settles much faster than Integral Absolute Error (IAE) and Integral Square Error (ISE). Integral Time Square Error (ITSE) forces large controller output for small changes in the reference value and hence, makes it undesirable for the application of Load Frequency Control (LFC) [103]. The ITAE-based objective function is defined as:

$$min(J) = \int_0^{T_{sim}} [|(\Delta f_1)| + |(\Delta f_2)| + |(\Delta P_{tie})|] \times t \ dt \tag{4.15}$$

where, $|(\Delta f_1)|$ and $|(\Delta f_2)|$ are absolute values of frequency deviation in Area-1 and 2, respectively, $|(\Delta P_{tie})|$ is the absolute value of change in the tie-line power and T_{sim} is the simulation time period with constraints as:

$$K_{Pmin} \leq K_P \leq K_{Pmax}$$

$$K_{Dmin} \leq K_D \leq K_{Dmax}$$

where, K_{Pmin} and K_{Pmax} represent minimum and maximum limit, respectively, of the gain of the proportional controller, whereas, K_{Dmin} and K_{Dmax} represent minimum and maximum limit, respectively, for the gain of the derivative controller.

4.4 SIMULATED CASE STUDY

The 11-bus system considered in this work consists of two interconnected areas. Both areas have two generation units of 900MVA each. EV fleet of 500 vehicles was connected at bus 7 in Area-1. The plug-in state of each EV was decided by the type of category they fall into, while SOC was initialized using the Gaussian distribution function with 85% average SOC and 10% standard deviation. For the estimation of EV's response to the frequency event, two different types of disturbance were simulated:

4.4.1 The disturbance caused by simulating fault

To simulate a frequency event, Line to Ground fault in phase-A was carried out at bus 8 in Line B, as shown in Fig. 4.9, at time t=20sec.

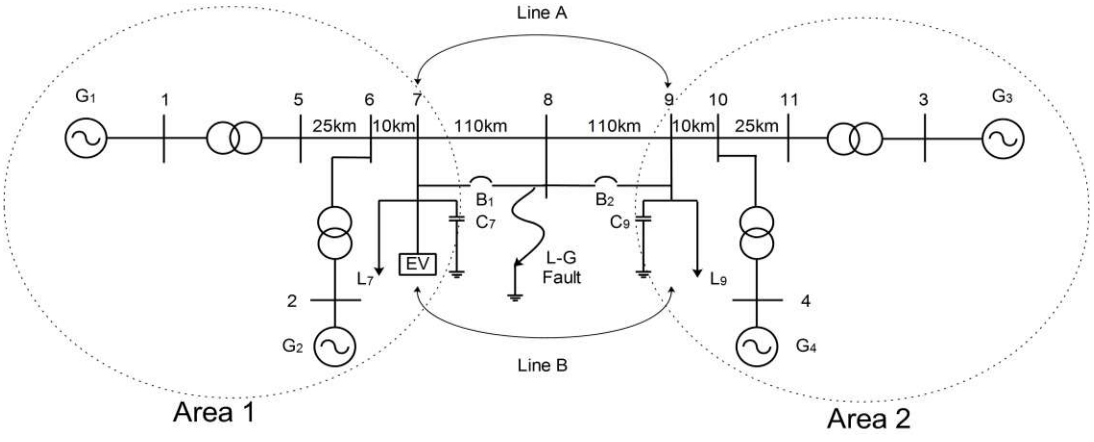

Fig. 4.9 Disturbance created using LG fault in the two-area system.

4.4.2 The disturbance caused by the change in reference power

Referring to Fig. 4.10, the mechanical power input to the generator G_1, in Area-1, was reduced to 0.9 p.u. at t=30sec and brought back to 1 p.u. at t=120sec.

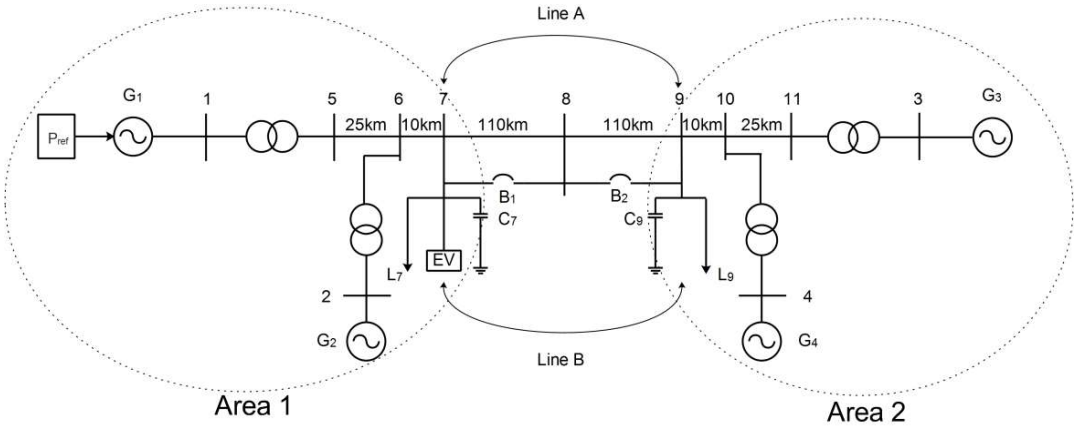

Fig. 4.10 Disturbance created using change in reference power in the two-area system.

The process flow for EVs participating in frequency regulation is shown in Fig. 4.11. In both the cases simulated, the total number of EVs was set to 500. For a frequency increase/drop greater than 0.5×10^{-3} Hz and SOC in between 85 to 95%, the number of EVs available for frequency regulation $N_{b\,reg}$ was calculated, and regulation power P_{reg} is calculated, thereafter.

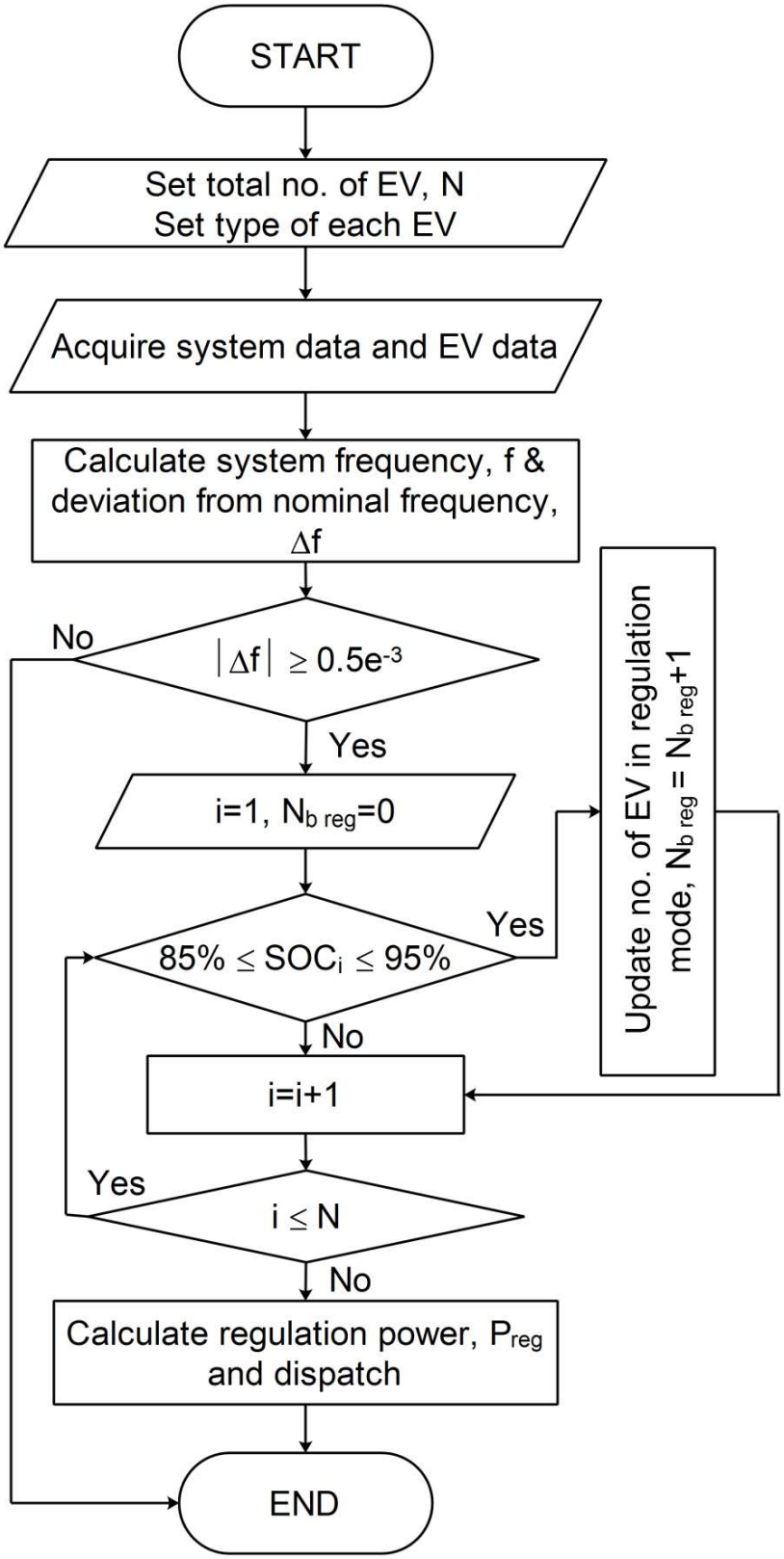

Fig. 4.11 Flowchart showing the process flow for EV's contribution in frequency regulation.

4.5 RESULTS AND DISCUSSION

4.5.1 The disturbance caused by simulating fault

Fig. 4.12 shows the over-frequency event with the steady-state frequency deviation of -0.35Hz at bus 7 (in Area-1) and 9 (in Area-2) for the L-G fault simulated at 20sec in phase A. The response of the EV in limiting the frequency deviation can be observed in Fig. 4.13, and voltage, current and active power absorbed by the EV during the frequency event is shown in Fig. 4.14. The continuous power dispatch by the EV fleet is in accordance with the steady-state frequency deviation. It can be seen further that the EV responds to the transients as well by injecting power into the grid.

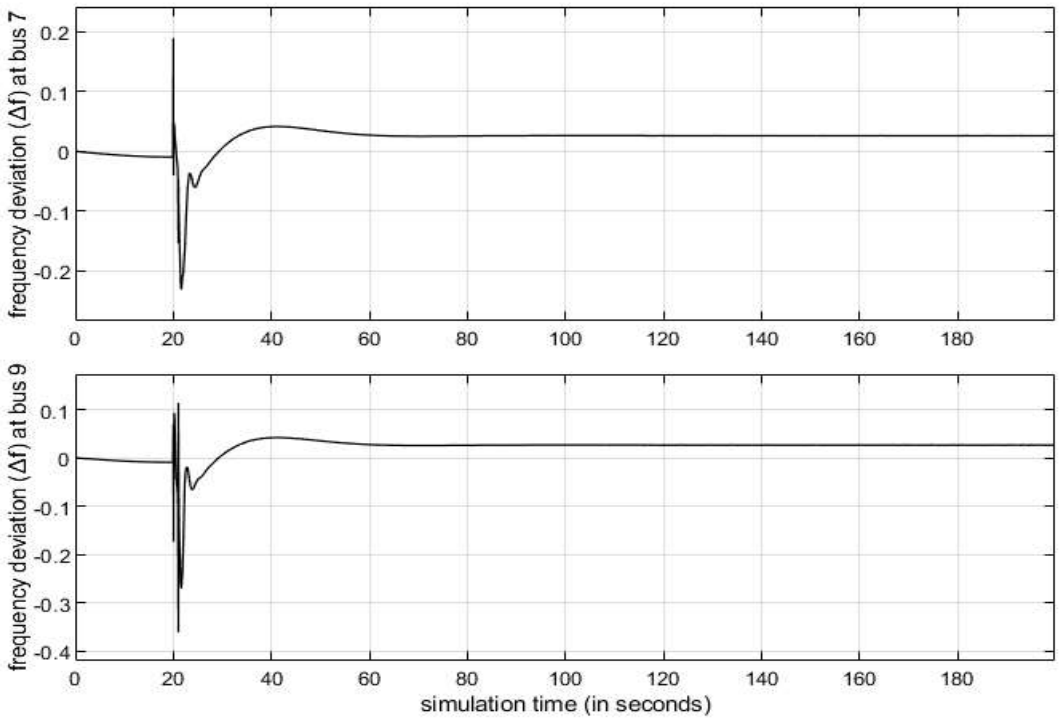

Fig. 4.12 Frequency deviations for disturbance without EV.

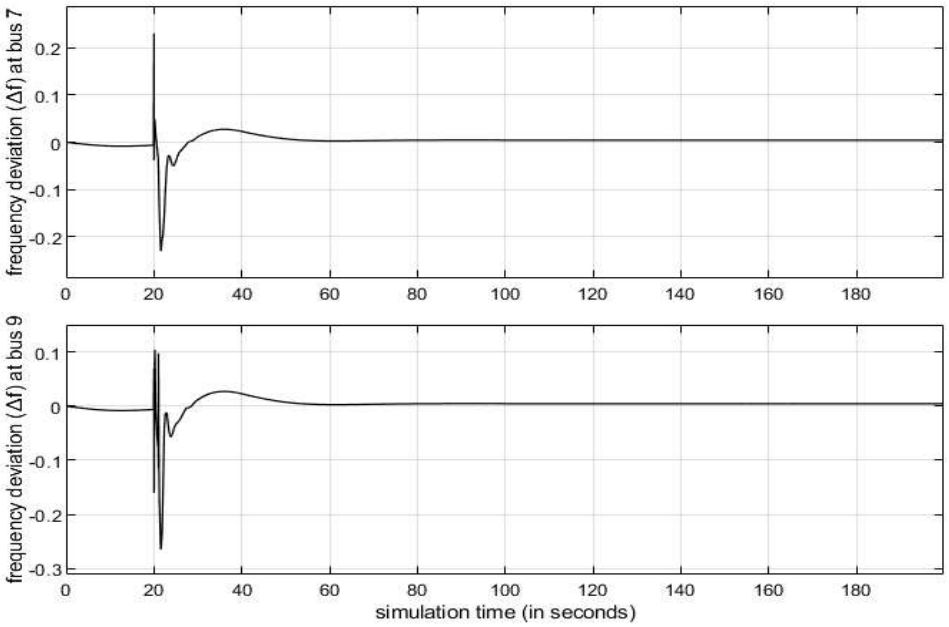

Fig. 4.13 Frequency deviations for a disturbance with EVs in frequency regulation mode.

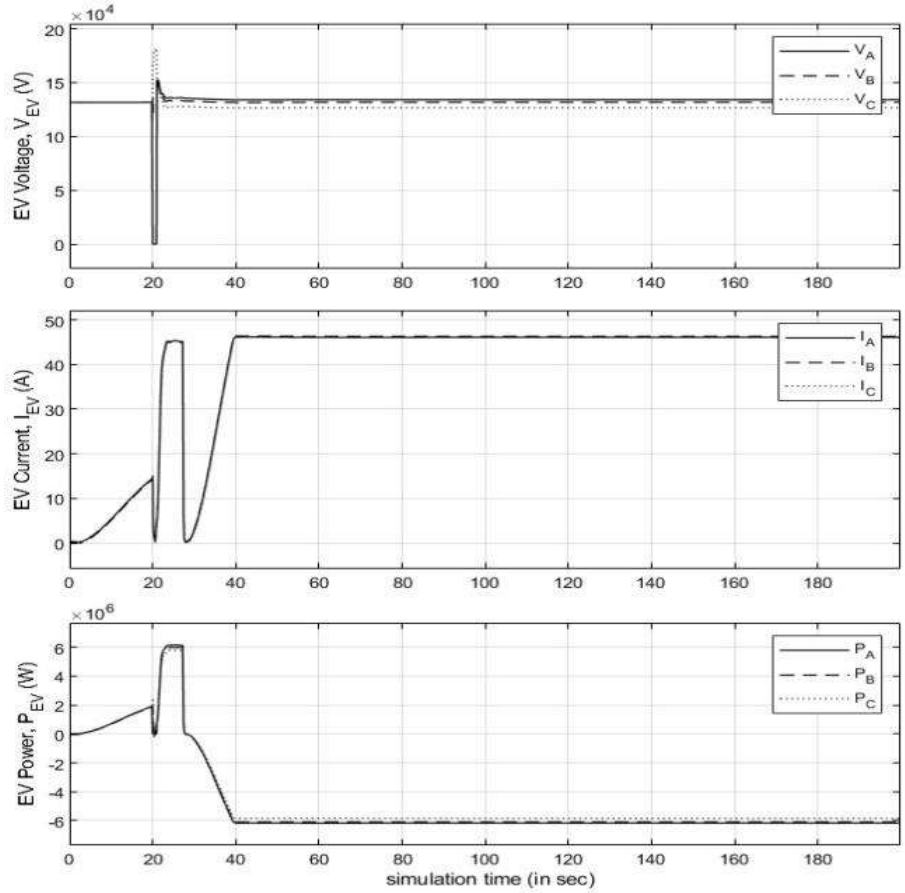

Fig. 4.14 Voltage, current and power of the EVs in frequency regulation mode.

The SOC of EVs falling under different categories is shown in Fig. 4.15. It is seen that EVs in Profile 1-4 are grid-connected and have SOC in between the range of 85-95%. Hence, they participate in frequency control and their SOC changes in accordance with the EV power. The EVs in Profile 5 are on a trip, i.e. grid disconnected; hence, their SOC is -100%. This value is chosen to differentiate between grid-connected EVs with 100% SOC and on-trip EVs with 100% SOC.

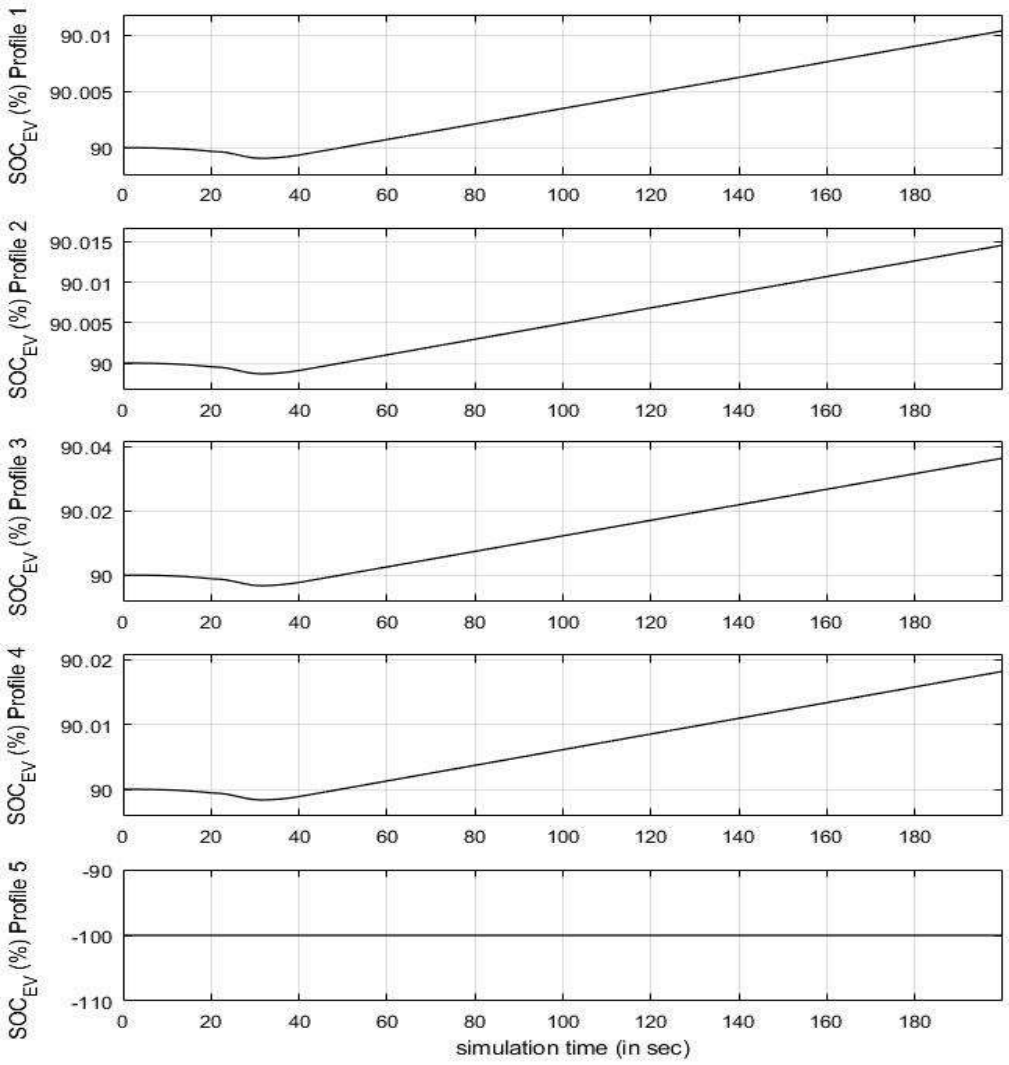

Fig. 4.15 SOC of the various EV profiles while performing frequency control.

4.5.2 The disturbance caused by a change in reference power

In this scenario, the frequency event is simulated by dropping the reference power input to the generator G_1 in Area-1 to 0.9p.u. at 30sec. As shown in Fig. 4.16, the frequency deviation at bus 7 and 9 is -0.08Hz. At 120sec, the reference power is brought back to 1p.u., and frequency restores to the pre-disturbance value.

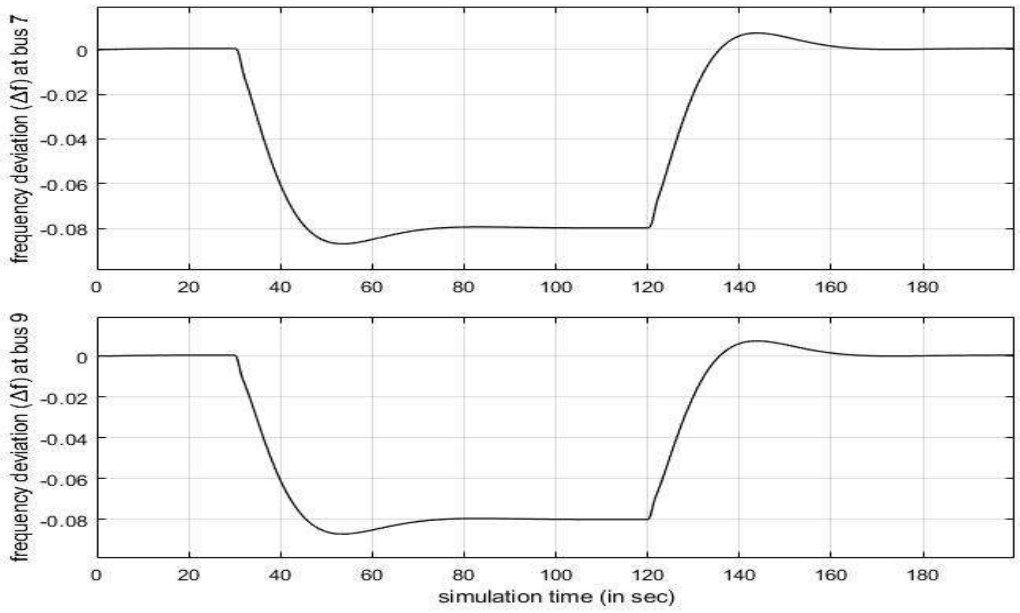

Fig. 4.16 Frequency deviations for disturbance without EV.

As shown in Fig. 4.17, the primary frequency response of EVs limits the frequency deviation to -0.065Hz, which corresponds to an 18.75% reduction in frequency deviation. The voltage, current and active power absorbed by the EV during the frequency event are shown in Fig. 4.18.

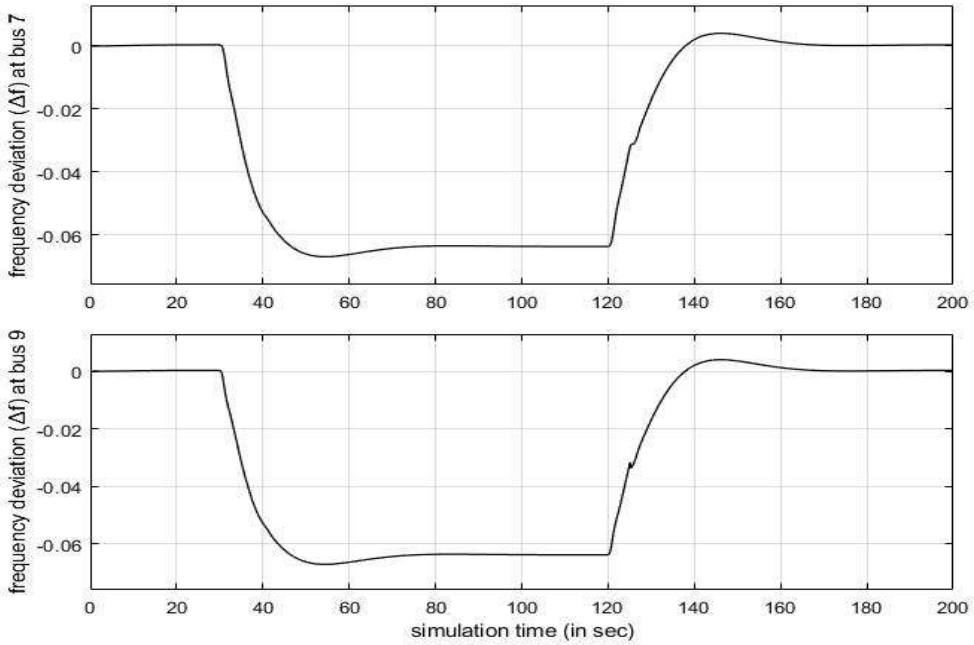

Fig. 4.17 Frequency deviations for a disturbance with EVs in frequency regulation mode.

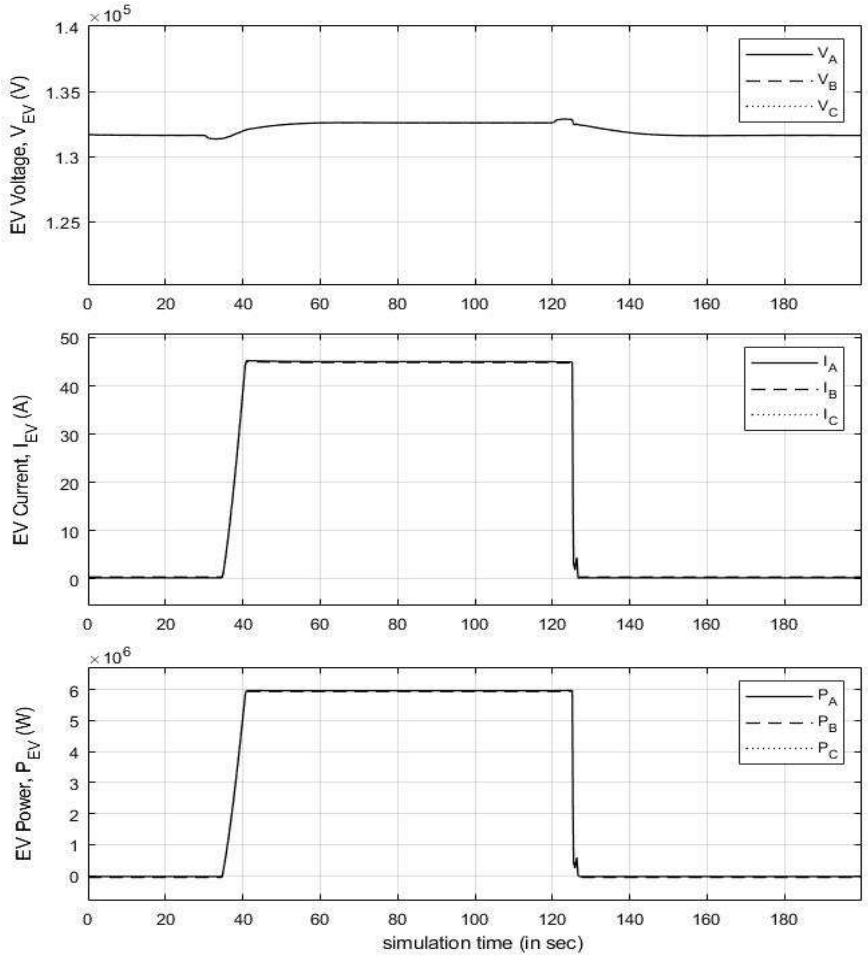

Fig. 4.18 Voltage, current and power of the EVs in frequency regulation mode.

It can be observed that the EVs have a very quick response to the frequency deviation and fall back to their initial consumption as soon as the system stabilizes. The SOC of various EV Profiles is shown in Fig. 4.19. During the under-frequency event, EVs in Profile 1-4 inject power into the grid; hence, the SOC falls in the period. EVs in Profile 5 are disconnected from the grid; hence, they do not participate in frequency regulation.

As described in Sub-section 4.2.3, the simulation results obtained fall under the category of Case B, whereby there is no intersection between critical frequency line $f = f_{cr}$ and system frequency curve. The values obtained for modified TFDI, η are shown in Table 4.4 with the nominal frequency of the system, $f_N = 50$Hz and critical system frequency, $f_{cr} = 49.5$Hz. The value of modified TFDI, η lies between 1 and 2, i.e., $1 \leq \eta \leq 2$, wherein a value closer to 2 is favourable. As can be observed from Table 4.4, there has been a significant rise in the value of modified TFDI, η at bus 9, whereas it remains nearly constant at bus 7 in the presence of the EV fleet for the fault case scenario. Whereas for the case simulated through a change in reference power of generator G_1 in Area-1, there is a marginal increase in η at both the buses, i.e., bus 7 and bus 9, in the presence of EVs. As frequency regulation through the EV fleet increases TFDI for bus 9 for both the cases and for bus 7 for Case-B, the EV fleet is capable of security margin enhancement, too.

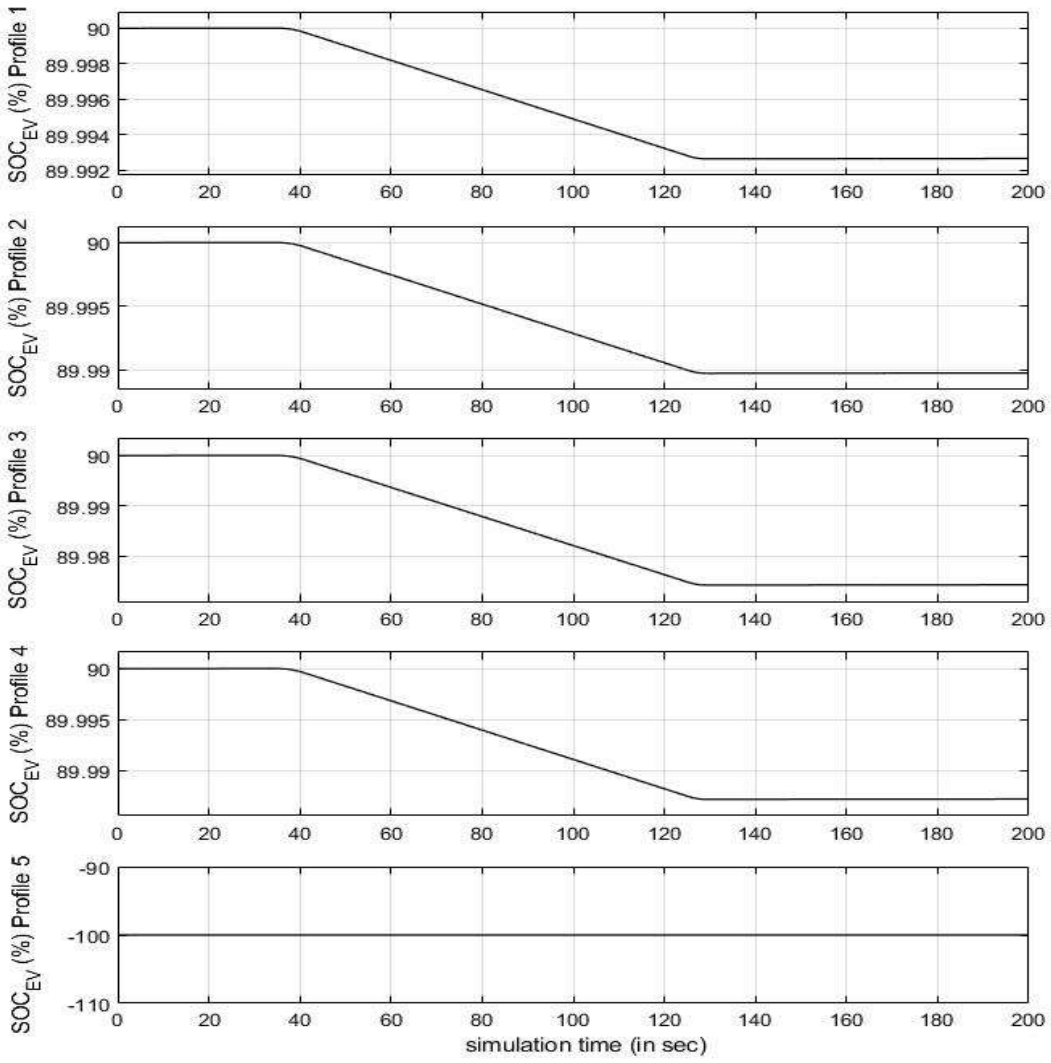

Fig. 4.19 SOC of the various EV profiles while performing frequency control.

Table 4.4 Frequency Nadir, ROCOF and TFDI without and with EVs for the different contingencies.

		Frequency Nadir, f (Hz)		ROCOF (Hz/s)		Transient Frequency Deviation Index, η		Percent increase in TFDI with EVs
		Without EVs	With EVs	Without EVs	With EVs	Without EVs	With EVs	
Case A: Fault	Bus 7	49.77	49.77	-0.15	-0.07	1.54	1.54	0
	Bus 9	49.65	49.73	-0.36	-0.11	1.3	1.46	12.3
Case B: ΔP_{ref}	Bus 7	49.92	49.935	-0.004	-0.003	1.84	1.87	1.6
	Bus 9	49.92	49.935	-0.004	-0.003	1.84	1.87	1.6

4.6 SUMMARY

In this research work, control of frequency deviations through EV charging power adjustment has been proposed. Further, EVs are utilized to stabilize the frequency deviations in the system. A control strategy is presented in order to determine the regulation power for bi-directional power flow by EVs in accordance with the frequency deviation. Distinct contingencies have been simulated to observe their effect on system frequency and the role of EVs in the mitigation of frequency deviations. To demonstrate the proposed scheme, aggregated EV fleet model is developed in SIMULINK. Further, a frequency deviation index, i.e. TFDI, was used to assess the depth of frequency deviation and improvement in its value is manifested for the case where EVs provide support in the mitigation of frequency deviation. The frequency regulation can be even more effective in the presence of more number of EVs in the fleet as more regulation power will be available during the contingency.